Connections between centrifugal, stratorotational, and radiative instabilities in viscous Taylor-Couette flow

Colin Leclercq,[1,*] Florian Nguyen,[1,2] and Rich R. Kerswell[1]
[1]*Department of Mathematics, University of Bristol, University Walk, Bristol BS8 1TW, United Kingdom*
[2]*École Normale Supérieure, Paris, France*
(Received 1 July 2016; published 6 October 2016)

The "Rayleigh line" $\mu = \eta^2$, where $\mu = \Omega_o/\Omega_i$ and $\eta = r_i/r_o$ are respectively the rotation and radius ratios between inner (subscript i) and outer (subscript o) cylinders, is regarded as marking the limit of centrifugal instability (CI) in unstratified inviscid Taylor-Couette flow, for both axisymmetric and nonaxisymmetric modes. Nonaxisymmetric stratorotational instability (SRI) is known to set in for anticyclonic rotation ratios beyond that line, i.e., $\eta^2 < \mu < 1$ for axially stably stratified Taylor-Couette flow, but the competition between CI and SRI in the range $\mu < \eta^2$ has not yet been addressed. In this paper, we establish continuous connections between the two instabilities at finite Reynolds number Re, as previously suggested by Le Bars and Le Gal [Phys. Rev. Lett. **99**, 064502 (2007)], making them indistinguishable at onset. Both instabilities are also continuously connected to the radiative instability at finite Re. These results demonstrate the complex impact viscosity has on the linear stability properties of this flow. Several other qualitative differences with inviscid theory were found, among which are the instability of a nonaxisymmetric mode localized at the outer cylinder without stratification and the instability of a mode propagating against the inner cylinder rotation with stratification. The combination of viscosity and stratification can also lead to a "collision" between (axisymmetric) Taylor vortex branches, causing the axisymmetric oscillatory state already observed in past experiments. Perhaps more surprising is the instability of a centrifugal-like helical mode beyond the Rayleigh line, caused by the joint effects of stratification and viscosity. The threshold $\mu = \eta^2$ seems to remain, however, an impassable instability limit for axisymmetric modes, regardless of stratification, viscosity, and even disturbance amplitude.

DOI: 10.1103/PhysRevE.94.043103

I. INTRODUCTION

There has been considerable recent interest in the effects of axial stratification on the Taylor-Couette problem following the discovery in 2001 [1,2] that it leads to instabilities outside the centrifugally unstable region. This region is conventionally defined by Rayleigh criterion [3] as

$$\mu < \eta^2, \quad \text{where} \quad \mu := \Omega_o/\Omega_i \quad \text{and} \quad \eta := r_i/r_o \qquad (1)$$

are respectively the rotation and radius ratios between inner and outer cylinders (denoted with indices i and o, respectively). Rayleigh derived his criterion for axisymmetric perturbations in the inviscid limit and only comparatively recently has it been extended to nonaxisymmetric, inviscid perturbations [4], albeit only in the limit of large axial wave numbers. Using an inviscid, small-gap analysis, Refs. [1,2] uncovered nonaxisymmetric stratified instabilities that could develop when the inner cylinder rotates faster than the outer one, despite the radial decrease in angular momentum: the so-called quasi-Keplerian regime, $\eta^2 < \mu < 1$. The new instability—later called the *stratorotational instability* or SRI in Ref. [5]—was interpreted as a resonance between boundary-trapped inertia-gravity waves. Using the same asymptotic framework as Ref. [4], Ref. [6] later showed that the SRI can become a radiative instability (RI) in the limit of an infinite gap ($\eta \to 0$) so that the outer boundary "goes to infinity." The RI mechanism relies on a critical layer to extract energy from the base flow and radiate an evanescent wave radially outwards. More recently, Ref. [7] extended the instability range of stratified Taylor-Couette flow even further, reaching the striking conclusion that the flow is *always* unstable, except for the special case of solid-body rotation, $\mu = 1$. Importantly, Ref. [7] relaxed the small-gap assumption initially made in Refs. [1,2] (by using large axial wave number asymptotics) and uncovered the role played by a critical layer to achieve over-reflection between the two boundary-trapped waves causing SRI.

With the exception of Ref. [8], pre-2001 laboratory experiments on stratified Taylor-Couette flow were always carried out with a fixed outer cylinder [8–12] (so $\mu = 0 < \eta^2$) and the relevance of the Rayleigh line was not questioned. The first experimental evidence of the SRI came in 2007 [13], when nonaxisymmetric instability was clearly observed in the centrifugally stable regime. Significantly, Ref. [13] explored a large range of rotation ratios and suggested a continuous connection between nonaxisymmetric modes dominating on each side of the Rayleigh line. In contrast, Ref. [6] claimed later that stratorotational instabilities (SRI and RI) are much weaker than the centrifugal instability (CI) when $\mu < \eta^2$, implying that (a) SRI, RI and CI are distinct, and (b) CI is always stronger. A distinction between SRI, RI and CI certainly exists in the inviscid limit (the optimal axial wave number is bounded for the SRI and RI [6,7], whereas it is not for the CI [4]) but this may not extend to the finite Reynolds numbers achievable in experiments (consistent with Ref. [13]). Certainly having this distinction (a) simplifies the identification of which instability mechanism dominates at a given point in parameter space but is not guaranteed. Also, plausibly, CI might exist beyond the Rayleigh line in the presence of stratification (consistent with Ref. [13]). To add to the uncertainty, statement (b) seems inconsistent with the findings of Ref. [14], which showed that

*c.leclercq@bristol.ac.uk

a RI could grow faster than a CI in the case of a stably stratified Rankine vortex in a rotating frame.

The purpose of this paper is to shed some light on these seemingly contradictory statements by carrying out a stability analysis of stratified Taylor-Couette flow which bridges the gap between experimentally relevant Reynolds numbers and large Reynolds numbers where inviscid analysis should hold in some fashion. The motivation for this study comes from an ongoing program of experimental work [15–17] and the desire to be able to interpret the mechanistic origin of the instabilities observed there. The key questions to be addressed are as follows:

(1) Are CI and SRI continuously "connected" (defined at the end of Sec. III) in parameter space or are they always distinct and thereby represent different instability mechanisms?
(2) Can SRI every dominate CI in the centrifugally unstable region $\mu < \eta^2$?
(3) Can CI exist for $\mu > \eta^2$ and therefore beyond the Rayleigh line with stratification?

Viscous linear analyses already exist in the literature, starting with the contribution of Ref. [18] based upon numerous simplifying assumptions. Reference [12] considered axisymmetric perturbations only (small-gap limit and finite gap but no density diffusion) while Refs. [1,19,20] considered the general case albeit only close to the marginal stability curve. Here the focus is to consider the dispersion relation for linear viscous disturbances over several decades of the Reynolds number up from the marginal stability curve to at least $O(10^4)$ and sometimes $O(10^{10})$. A large range of rotation ratios is also considered in order to assess the relevance of the Rayleigh line $\mu = \eta^2$ at finite Re and with stratification.

The plan of the paper is as follows. In Sec. II, we briefly introduce the governing equations and numerical methods. In Sec. III, we present the results of our parametric stability analysis and discuss the effect of the different control parameters on the dominant mode. In Sec. IV, we assess the connection between CI and SRI at finite Re by exploring the discontinuities of the optimal axial wave number in the (μ,Re) plane. By doing so, we reveal several connections between the different instabilities and show the limits of Rayleigh criterion in viscous stratified Taylor-Couette flow. We summarize our findings in Sec. V.

II. PROBLEM FORMULATION

A. Governing equations

The geometry of an axially infinite container is characterized by the radius ratio η, while rotation and shear are jointly characterized by the rotation ratio μ [see Eq. (1)] and Reynolds number Re, which is defined as

$$\mathrm{Re} := \frac{r_i \Omega_i (r_o - r_i)}{\nu} \tag{2}$$

with ν the kinematic viscosity. The purely azimuthal basic velocity profile $\mathbf{U} := r\Omega(r)\hat{\boldsymbol{\theta}}$ is of the form

$$\Omega(r) := A + \frac{B}{r^2}, \tag{3}$$

with $A := (\mu - \eta^2)/[\eta(1+\eta)]$ and $B := \eta(1-\mu)/[(1+\eta)(1-\eta)^2]$. The basic density profile $\bar{\rho}(z)$ is linear in the axial direction z and characterized by a constant buoyancy frequency $N := \sqrt{-(g/\rho_0)d\bar{\rho}/dz}$, based on gravity g and a reference density ρ_0. Two nondimensional parameters characterize stratification: the Richardson and Schmidt numbers

$$\mathrm{Ri} := \frac{N^2}{\Omega_i^2} \quad \text{and} \quad \mathrm{Sc} := \frac{\nu}{\kappa}, \tag{4}$$

where κ is the diffusivity of mass. For all the results presented in this paper, the Schmidt number was set to a value of 700 appropriate for salt-in-water experiments [15–17] with only a few exploratory calculations done with $\mathrm{Sc} = 7$ appropriate for heated-water experiments (see later in Sec. V). In the following, we take $d := r_o - r_i$ as the unit of length, $r_i\Omega_i$ as the unit of speed, and $\rho_0 N^2 (r_o - r_i)/g$ as the unit of density.

We consider the dynamics of infinitesimal perturbations of the velocity $\mathbf{u}' = u'\hat{\mathbf{r}} + v'\hat{\boldsymbol{\theta}} + w'\hat{\mathbf{z}}$ in cylindrical coordinates, pressure p' and density ρ', around the linearly stratified basic flow (3). Perturbations can be written in the form of normal modes

$$(u', v', w', p', \rho') = [u(r), v(r), w(r), p(r), \rho(r)] e^{i(kz + m\theta - \omega t)}$$

with complex frequency ω, integer azimuthal wave number m, and real axial wave number k. In the Boussinesq approximation, the linearized incompressible Navier-Stokes, advection-diffusion, and continuity equations read

$$isu - 2\Omega v + d_r p = \frac{1}{\mathrm{Re}}\left(\nabla^2 u - \frac{u}{r^2} - \frac{2im}{r^2} v\right), \tag{5}$$

$$isv + Zu + \frac{im}{r} p = \frac{1}{\mathrm{Re}}\left(\nabla^2 v - \frac{v}{r^2} + \frac{2im}{r^2} u\right), \tag{6}$$

$$isw + ikp = -\mathrm{Ri}^*\,\rho + \frac{1}{\mathrm{Re}}\nabla^2 w, \tag{7}$$

$$is\rho - w = \frac{1}{\mathrm{Re}\,\mathrm{Sc}}\nabla^2 \rho, \tag{8}$$

$$0 = \frac{1}{r} d_r (ru) + \frac{im}{r} v + ikw, \tag{9}$$

where $\mathrm{Ri}^* := \mathrm{Ri}[(1-\eta)^2/\eta^2]$, $s := m\Omega - \omega$ is the Doppler-shifted frequency, $Z := (1/r)d(r^2\Omega)/dr$ is the axial vorticity of the basic flow, and $\nabla^2 = d_{rr}^2 + (1/r)d_r - (k^2 + m^2/r^2)$. The boundary conditions are no slip ($u = v = w = 0$) and no flux $d_r\rho = 0$ at the walls. Symmetries are such that $\omega(k,m) = \omega(-k,m) = -\omega^\star(-k,-m)$, where * denotes the complex conjugate. Therefore, we consider only positive k and m without loss of generality.

B. Numerical methods

The governing equations were discretized using Chebyshev collocation in the radial direction, leading to a generalized eigenvalue problem for ω and (u,v,w,p,ρ). This problem was solved using multithreaded LAPACK routines with OPENBLAS. The number of Chebyshev polynomials used for each dependent variable was set to 140 for calculations below $\mathrm{Re} = 1 \times 10^4$ and increased up to a maximum of 480 when required at higher Re (at $(\mathrm{Re},\mu,\eta,Sc,m) = (10^4,0,0.417,700,1)$ and $\mathrm{Ri} \in \{0.25,4,25\}$, doubling the resolution from 140 to 280 led to less than 1% variation in the growth rate of the most unstable mode). The code was validated by reproducing Figs. 4 and 10

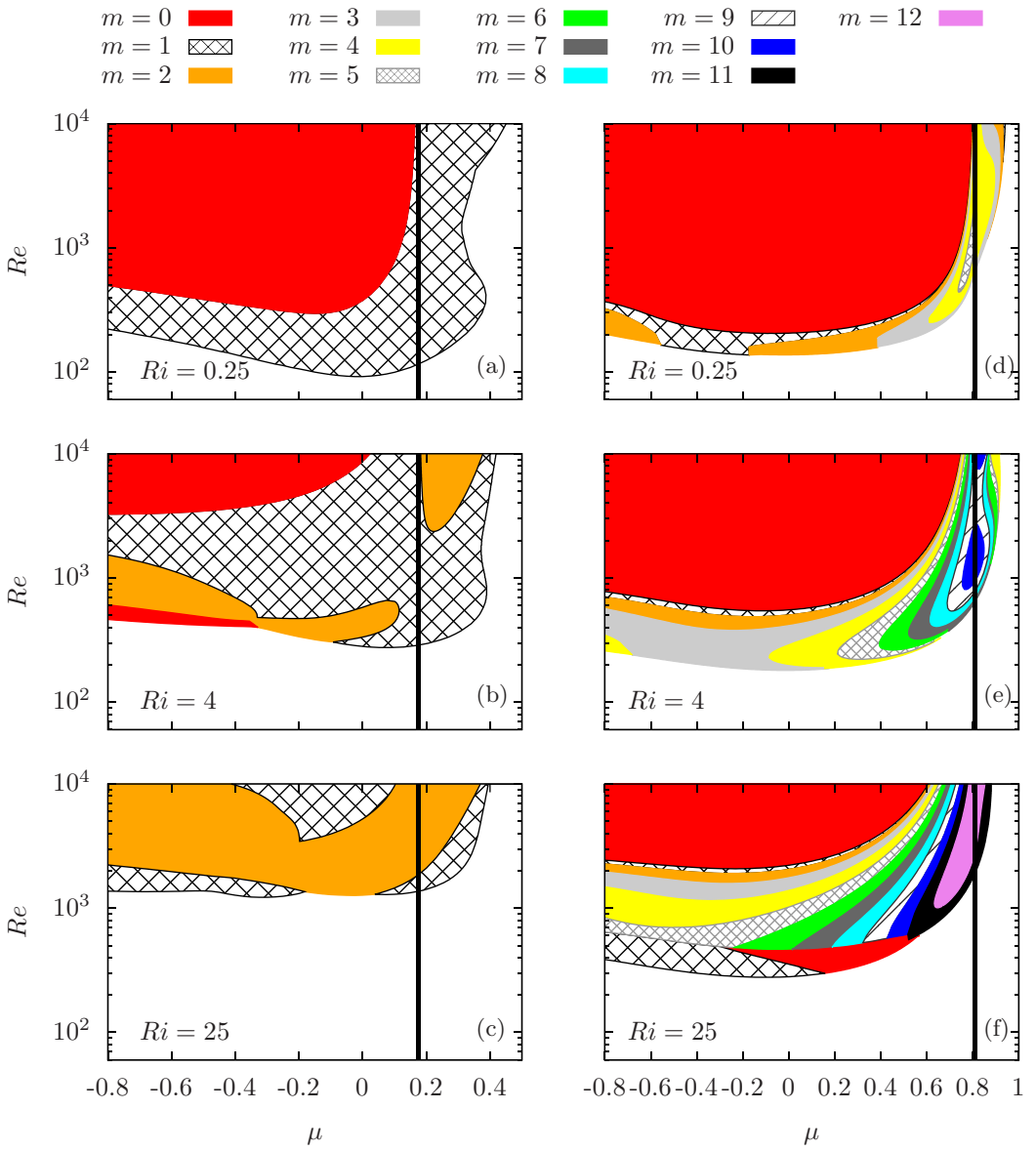

FIG. 1. Dominance diagrams showing the azimuthal mode number m of the fastest growing mode (growth rate optimized over k) for (a)–(c) $\eta = 0.417$ and (d)–(f) $\eta = 0.9$ and Ri $= 0.25$, 4, and 25 (indicated in the plot). The thick black line indicates the Rayleigh line.

from Ref. [7]. For a given m, the most unstable mode was found by optimizing the growth rate over k, using a Newton-Raphson method. Standard continuation methods were used to follow local maxima of the growth rate in parameter space.

III. DOMINANCE DIAGRAMS

We start by presenting the azimuthal mode number of the fastest growing mode in the (μ,Re) plane, for three values Ri $= 0.25$, 4, and 25 and two radius ratios: a "large"-gap case $\eta = 0.417$ (used in Refs. [15–17]) and a "small"-gap case $\eta = 0.9$. The dominant m was obtained after optimization of the growth rate $\omega_i := \mathrm{Im}(\omega)$ over all possible sets of wave numbers $(m,k) \in \mathbb{N} \times \mathbb{R}^+$. Results are given in Fig. 1, for a large range of μ and Re $\leqslant 1 \times 10^4$. The vertical black line corresponds to the Rayleigh line $\mu = \eta^2$.

The first observation is the rise of the marginal stability curve to higher Re indicating the stabilizing effect of stratification for all μ and both η considered, consistent with previous results in the literature. The second common feature of all the plots is that axisymmetric ($m = 0$) steady vortices (hereafter referred to as Taylor vortices) only dominate in regions removed from the marginal stability curve. The $m = 0$ dominance regions near the marginal curve are distinct since they have nonzero frequency. These oscillatory $m = 0$ instabilities have already been found numerically in Refs. [19,21] and experimentally in Refs. [11,12], but were not apparently seen in Ref. [13] presumably because of their very restricted domain of dominance. Indeed, the critical instability is most often nonaxisymmetric, with larger m values becoming preferred as Ri increases. In the small-gap case, the effect of the Rayleigh line is clearly visible: the dominant m peaks to a maximum in its vicinity and decreases on both sides. For the large-gap case though, only $m = 0, 1, 2$ values dominate, and the Rayleigh line only seems to mark the limit of the dominant steady $m = 0$ region.

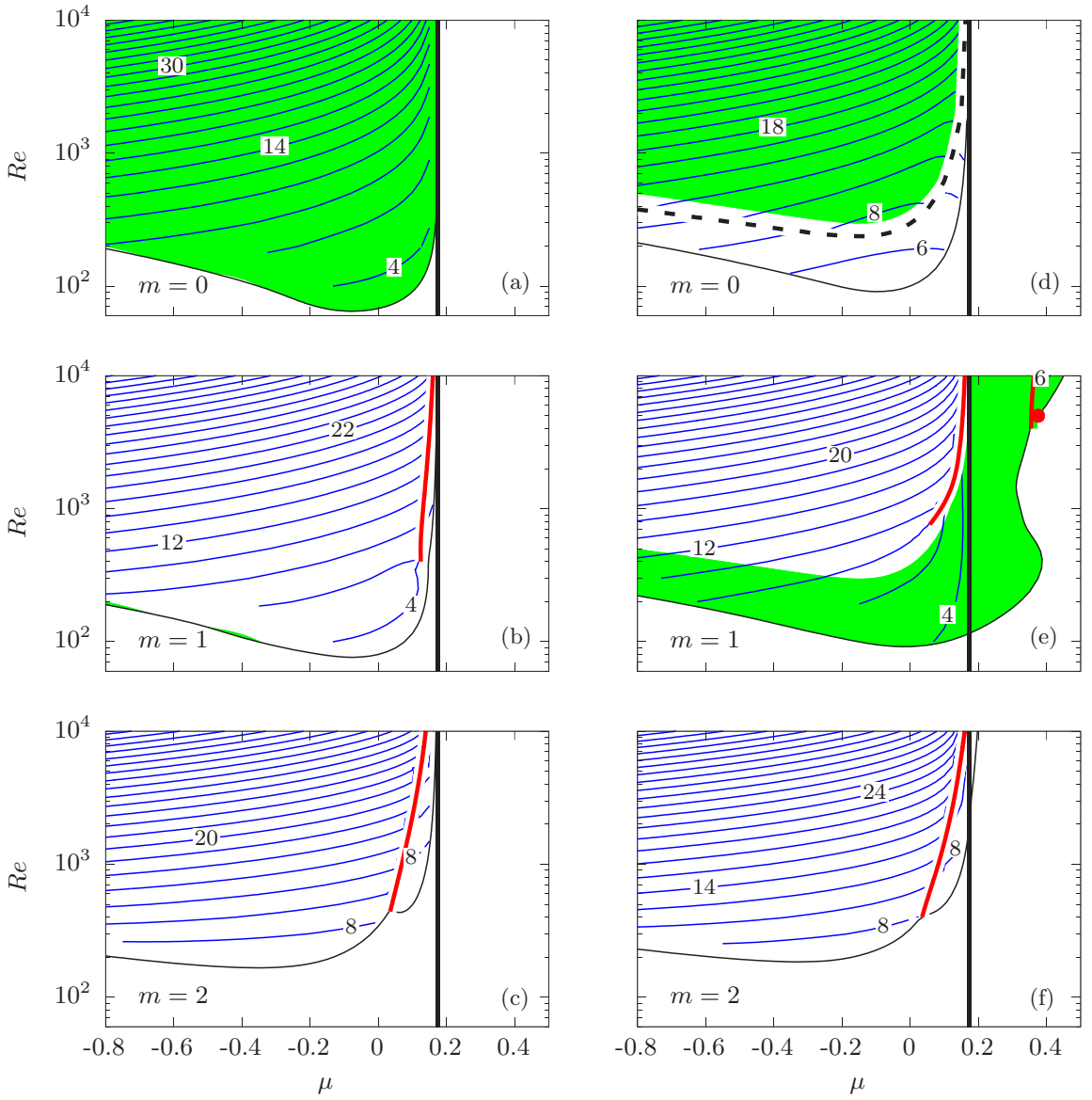

FIG. 2. Contours of optimal axial wave number $k_{\max}$ in the instability zone of modes $m = 0$, $m = 1$, and $m = 2$ for $\eta = 0.417$ and (a)–(c) $\mathrm{Ri} = 0$, (d)–(f) $\mathrm{Ri} = 0.25$. The spacing between contours is $\Delta k_{\max} = 2$ and the maximum is always in the top left corner. The Rayleigh line $\mu = \eta^2$ is indicated by a thick black line. Discontinuities in $k_{\max}$ are indicated by thick red curves. Dashed curves for $m = 0$ indicate a transition from an oscillatory (below) to a steady mode (above). The shaded regions indicate dominance of the given mode among all m (note the dominance of $m = 1$ in a very narrow range of parameter space for $\mathrm{Ri} = 0$ and $\mu \in [-0.8, -0.4]$). Finally, the dot in the $(m,\mathrm{Ri}) = (1,0.25)$ plot indicates the parameter values for the calculation of the eigenmode shown in Fig. 8(b).

The dominance diagrams show the existence of disconnected patches and kinks in their boundaries (e.g., for $m = 2$, $\eta = 0.417$, and $\mathrm{Ri} = 4$). These features suggest that different instabilities corresponding to the same value of m are competing for dominance. In order to assign an instability mechanism to each dominant mode, we track the loci of the discontinuities of $k_{\max}$—the axial wave number maximizing the growth rate—over (μ,Re) space for every fixed m in the next section. A discontinuity in $k_{\max}$ indicates the coexistence of two global maxima in the growth rate curve $\omega_i(k)$ (defined as the maximum growth rate at a *given* k): on either side of it, the maxima switch dominance, giving rise to the discontinuity in $k_{\max}$. If this discontinuity always separates the two competing instabilities in parameter space we refer to them as being *distinct* instabilities having different mechanisms. Conversely, if at some point the discontinuity terminates, indicating that the local maxima have merged, we consider the two instabilities as being continuously *connected* in parameter space and therefore not distinct. (Formally, there is also the possibility that two distinct instabilities cross over, momentarily having the same ω_i at $k_{\max}$, but this would give rise to a discontinuity in ω_r which is never seen in this study.)

IV. EXPLORING THE DISCONTINUITIES OF THE OPTIMAL AXIAL WAVE NUMBER IN THE (μ,Re) PLANE

Figures 2 and 3 break down each dominance diagram into contributions from $m = 0,1,2$ in the large-gap case. We

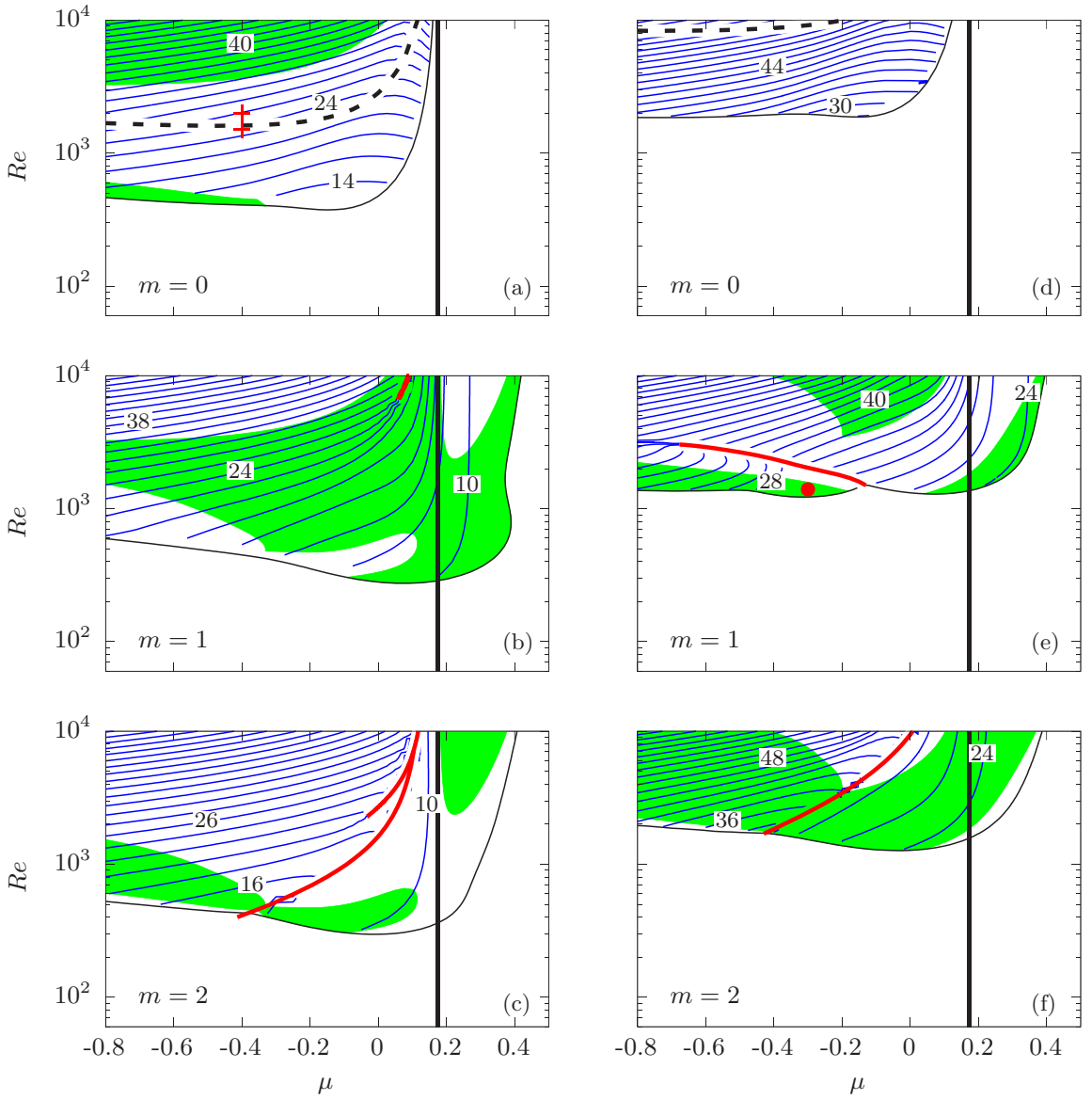

FIG. 3. Same as Fig. 2 but for (a)–(c) Ri = 4 and (d)–(f) Ri = 25. The dot in the (m,Ri) = (1,25) plot indicates the parameter values for the calculation of the eigenmode shown in Fig. 8(a). The red crosses in the (m,Ri) = (0,4) plot indicate the parameter values used to generate Fig. 4.

plot the contours of $k_{\max}$, in order to identify the loci of the discontinuities for each m. The region where a given m dominates overall is shaded. Figure 2 compares the weakly stratified case (Ri = 0.25) to the unstratified one, while Fig. 3 compares the moderate (Ri = 4) and strong (Ri = 25) stratifications.

A. Oscillatory axisymmetric mode as a collision between Taylor vortex branches

For $m = 0$, there is no discontinuity in $k_{\max}$ but a dashed curve marks the limit between oscillatory (below the line) and steady axisymmetric vortices (above). For all values of Ri $\neq 0$, the critical $m = 0$ instability is always oscillatory, as already found by Refs. [18,21] at large enough Sc, but becomes subdominant to steady vortices at large enough Re. To understand this transition better, we plot in Fig. 4 the dependency of the frequencies ω_r and growth rates ω_i of the two dominant axisymmetric modes against k for two values of Re: one below the dashed curve (Re = 1500) and one above (Re = 2000) (marked by red crosses in Fig. 3). This figure shows that the oscillatory vortices are created as Re decreases from 2000 by the collision between two steady vortex branches. This is clearly a joint effect of stratification and viscosity, as the "bubble" in Fig. 4(a) only appears if Re is small enough and Ri $\neq 0$.

B. Continuous connections between nonaxisymmetric CI and SRI modes in the (μ,Re) plane

There are discontinuities in $k_{\max}$ for all nonaxisymmetric modes, including when Ri = 0, and these are indicated by

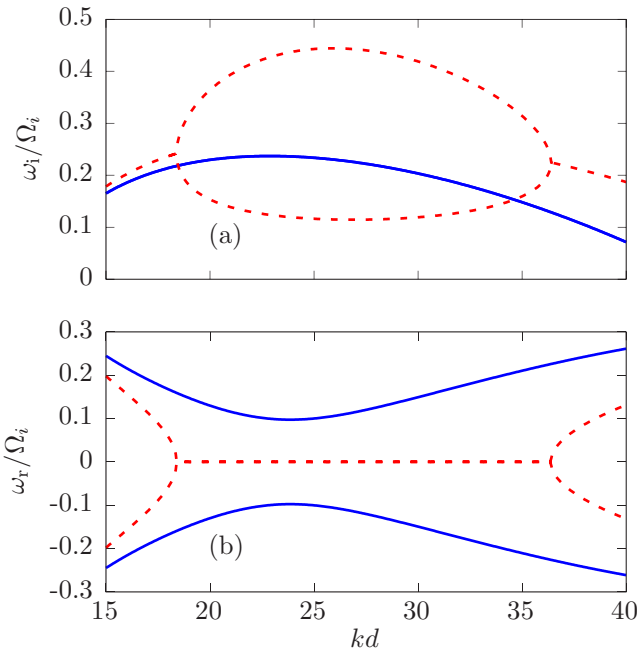

FIG. 4. (a) Growth rate and (b) frequency versus axial wave number k of the two most unstable $m = 0$ modes for $\mathrm{Ri} = 4$, $\mu = -0.4$, and $\mathrm{Re} = 1500$ (solid line) or $\mathrm{Re} = 2000$ (dashed line).

thick red curves in Figs. 2 and 3. For $m = 1$, the discontinuity near the Rayleigh line disappears within the unstable regions, at low enough Re, indicating that the instabilities on either side are smoothly connected. For $m = 2$, however, the discontinuity always seems to separate the instability region into two distinct zones. But tracking the discontinuity further up in Reynolds number in Fig. 5 shows that it terminates just above $\mathrm{Re} \approx 2 \times 10^5$ for $\mathrm{Ri} = 0.25$, indicating that the competing instabilities are again smoothly connected.

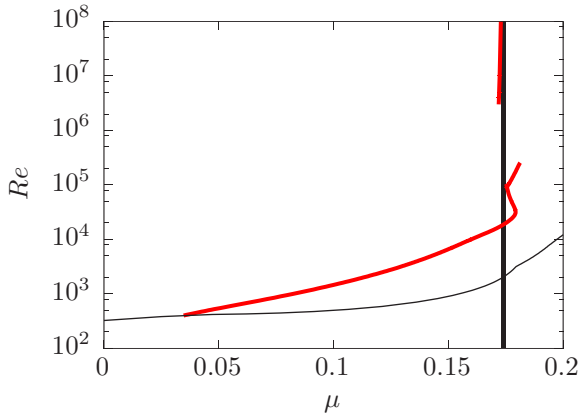

FIG. 5. Discontinuities of $k_{\max}$ in the (μ,Re) plane, for $\eta = 0.417$, $m = 2$, $\mathrm{Ri} = 0.25$, and $\mathrm{Re} \in [10^2, 10^8]$. As evident here, the discontinuity appearing in Fig. 2 below $\mathrm{Re} = 1 \times 10^4$ does not asymptote to the Rayleigh line as $\mathrm{Re} \to \infty$. In fact, for $2 \times 10^5 \lesssim \mathrm{Re} \lesssim 3 \times 10^6$ and $0.16 < \mu < 0.18$ there is no discontinuity at all in $k_{\max}$, which reveals, again, a continuous connection between CI and SRI at large, but finite Re. At even larger Re, a discontinuity reforms, permanently separating CI from SRI as $\mathrm{Re} \to \infty$.

At yet higher Re, a discontinuity reappears as it must do if the viscous analysis is to be consistent with inviscid predictions since there CI occurs at infinite k [4], whereas $k_{\max}$ remains finite for the SRI [7]. The value of μ where the growth rates of both instabilities are equal may be computed by suppressing the viscous term in the momentum equations (5)–(8) for the SRI, and using the analytical expression given in Ref. [4] for the CI in the inviscid limit (denoted with superscript ∞): $\omega^{\infty}_{i,\mathrm{CI}} = \sqrt{-\Phi(r_i)}$ (independent of m), where $\Phi := (1/r^3)d(r^4\Omega^2)/dr$ is the Rayleigh discriminant. We find that the switchover from SRI to CI dominant occurs at a value of μ which is very close to but below η^2. Indeed, $\omega^{\infty}_{i,\mathrm{CI}}$ exactly vanishes on the Rayleigh line, whereas $\omega^{\infty}_{i,\mathrm{SRI}}$ does not. Therefore, there is a very narrow range of $\mu < \eta^2$ where nonaxisymmetric SRI dominates CI in the inviscid limit. But this region is very small, which explains why Ref. [6] claimed that CI dominates over SRI in the centrifugally unstable region. By a continuation argument, a discontinuity in $k_{\max}$ must be found at large but finite Re, which asymptotes the inviscid value of μ where $\omega^{\infty}_{i,\mathrm{SRI}} = \omega^{\infty}_{i,\mathrm{CI}}$. The discontinuities for $m = 1$ in Figs. 2 and 3 seem to directly approach this limit as $\mathrm{Re} \to \infty$. For $m = 2$ and $\mathrm{Ri} = 0.25$, the discontinuity forming at $\mathrm{Re} \approx 3 \times 10^6$ also asymptotes the inviscid limit at larger Re. This analysis of the discontinuities of $k_{\max}$ in the (μ,Re) plane establishes the continuous connection between CI and SRI mechanisms at finite Re for $m = 1$ and $m = 2$.

C. A centrifugal instability mode localized at the outer cylinder in the unstratified case

A simple way to attempt to differentiate between CI and SRI is to suppress stratification: if the flow is stabilized, the instability was a SRI; otherwise it was a CI. This motivated us to compute the dispersion relation of modes $m = 0,1,2$ in the unstratified case as well. As shown in Fig. 2, there is no longer an instability beyond the Rayleigh line when $\mathrm{Ri} = 0$, but surprisingly, we still observe a discontinuity in $k_{\max}$ asymptoting $\mu = \eta^2$ at large Re for $m = 1$ and 2. This result was unexpected, as we previously associated such discontinuity to a CI and SRI competing in the inviscid limit. However, since SRI is caused by a resonance between boundary-trapped inertia-gravity waves [1,2], the mode dominating on the right of the discontinuity cannot be SRI when $\mathrm{Ri} = 0$. This suggests that this previously unreported CI branch on the right of the discontinuity for $\mathrm{Ri} = 0$ is connected to a SRI as Ri increases from zero. This new CI mode dominating to the right of the discontinuity is localized exclusively at the outer cylinder, as can be seen in Fig. 6(b) at $\mathrm{Re} = 1 \times 10^6$, whereas the one to the left of the discontinuity is localized at the inner cylinder [Fig. 6(a)]. These wall modes are reminiscent of the two families of neutral branches which create SRI in the inviscid limit [7]. In that limit, the outer-wall mode can only become unstable by coupling with the inner one, under the effect of stratification, but here we find that it may become unstable alone with the help of viscosity. Since the discontinuity in $k_{\max}$ asymptotes to the Rayleigh line as $\mathrm{Re} \to \infty$, this mode never dominates the inner-wall one in the inviscid limit: there is therefore no contradiction with the theoretical analysis of Ref. [4].

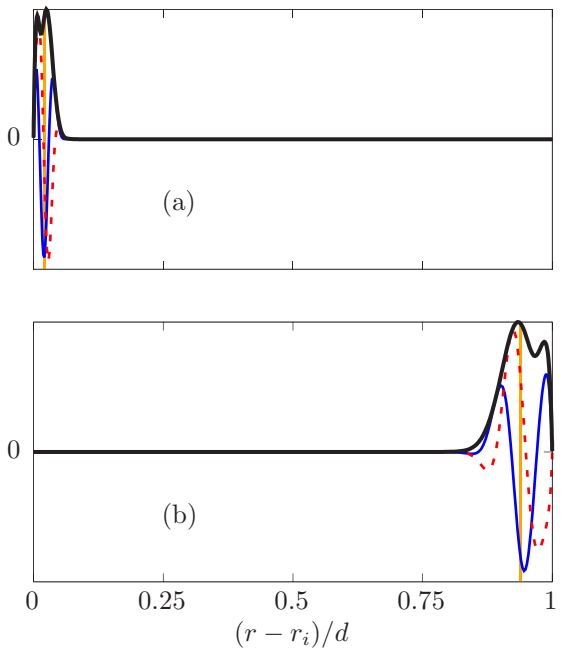

FIG. 6. Vertical velocity component of the two leading $m = 1$ eigenmodes at the discontinuity in $k_{\max}$ for $\mathrm{Re} = 1 \times 10^6$ and $\mathrm{Ri} = 0$: (a) left side of the discontinuity, (b) right side. Thin solid line, real part w_r; dashed line, imaginary part w_i; thick solid line, $|w|$. Points where $\Omega(r_t) - \omega = 0$ are indicated with a solid line at $r = \mathrm{Re}(r_t)$. These correspond to turning points in the Wentzel-Kramers-Brillouin (WKB) theories of RI [7] and SRI [6], but do not play any particular role in the asymptotic description of CI [4]. Here we show that these points indicate the position where the modes are localized at large Re.

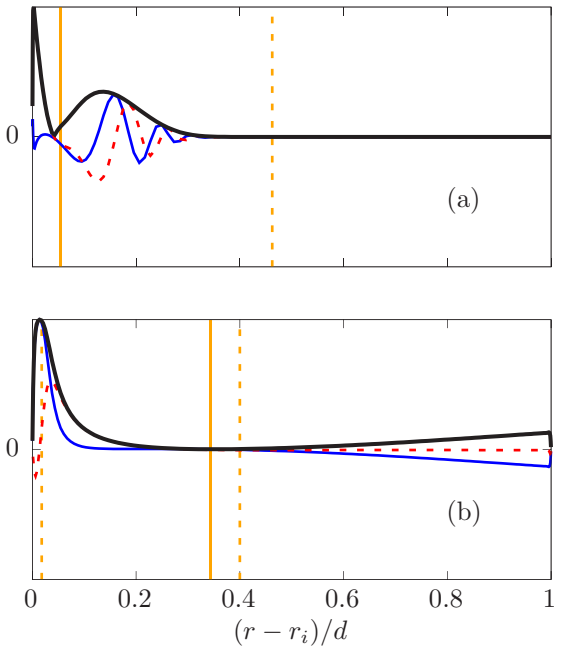

FIG. 7. Same as in Fig. 6, but for the leftmost discontinuity (near the Rayleigh line) in Fig. 2 for $(m,\mathrm{Ri}) = (1,0.25)$ and $\mathrm{Re} = 1 \times 10^6$. Here we also indicate the critical points $\Omega(r_c^{\pm}) - \omega = \pm N$ with dashed lines at $r = \mathrm{Re}(r_c \pm)$ [r_c^- is outside the domain in (a)].

D. Radiative instability mode connecting CI to SRI in finite gap

In Fig. 7, we compare the structure of the two modes on the discontinuity close to the Rayleigh line for $m = 1$, $\mathrm{Re} = 1 \times 10^6$, and $\mathrm{Ri} = 0.25$. The instability dominating to the left (decreasing μ) of the discontinuity must tend to a CI as $\mathrm{Re} \to \infty$, while the instability to the right must tend to a SRI. As a way of confirmation, the right branch has a structure which is reminiscent of inviscid SRI: the mode is localized at the walls and has a critical layer [see Fig. 7(b)], as described in Ref. [7]. However, since $k_{\max}$ remains small, the WKB framework of Ref. [7] does not obviously apply so there are not the oscillatory regions described by these authors.

The structure of the left branch, however, resembles the radiative instability mode described in Ref. [6] in the limit where the gap and Reynolds numbers become infinite, while $\mu \to \eta^2$ (and $kd \gg 1$). There is a critical layer and an oscillatory region of radially decaying amplitude in Fig. 7(a), similar to Fig. 3 in Ref. [6]. This region is bounded to the right by the critical point $\Omega(r_c^+) - \omega = N$, as in these authors' theory for weak stratification. This critical point effectively isolates the radiated wave from the outer cylinder, which may explain why we were able to find a RI mode in our finite-gap geometry, whereas Ref. [6] only refers to this instability in the limit of an infinite gap. In the present case, the RI seems to mediate the continuous morphing from the SRI to a CI at finite Re.

E. A helical mode propagating against the inner cylinder rotation

Finally, in the last two sections we investigate the nature of the modes in regions of the (μ,Re) plane created by unexpected discontinuities of $k_{\max}$, i.e., discontinuities that do not separate CI from SRI in the inviscid limit. First we discuss the critical $m = 1$ mode at large $\mathrm{Ri} = 25$ in the counter-rotating regime $\mu < 0$ (see the solid dot in Fig. 3). Surprisingly, the azimuthal velocity ω_r/m associated with that mode is negative, whereas it is always positive for other dominant modes. Such peculiar behavior has not been reported before. Inspecting the structure of this mode in Fig. 8(a) indicates that it is not a SRI, as the amplitude of $|w|$ is negligible near the outer wall. The turning point r_t such that $\Omega(r_t) - \omega = 0$ does not seem to coincide with any particular feature of the mode structure, confirming that asymptotic theories of CI, RI, and SRI are of little help at this low $\mathrm{Re} = 1400$. Because of the apparent absence of a critical layer, we conclude that the mode is best classed as a CI.

F. A centrifugal-type mode beyond the Rayleigh line destabilized by viscosity

Finally, we discuss the discontinuity located at the right of the Rayleigh line in Fig. 2 for $(m,\mathrm{Ri}) = (1,0.25)$. Since the dominant mode is "beyond" the Rayleigh line and well separated from the CI region by two discontinuities in $k_{\max}$, it is tempting to call this mode SRI. However, looking at the mode in Fig. 8(b) reveals a structure which is highly reminiscent

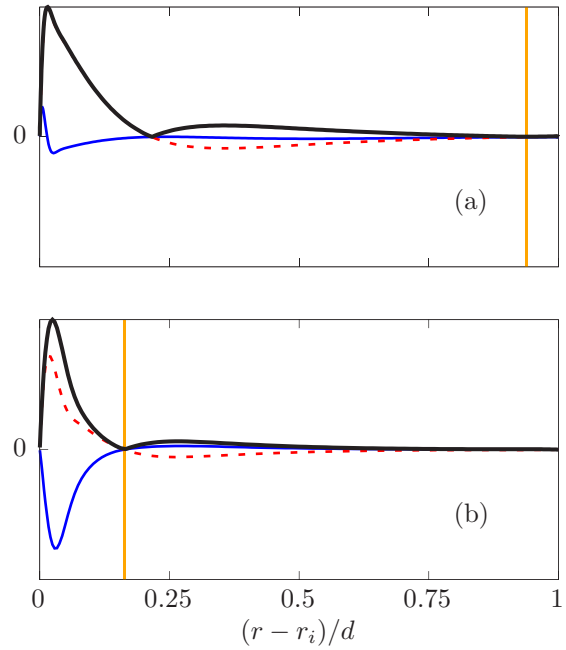

FIG. 8. Vertical velocity component of the leading eigenmodes at parameter values indicated by solid dots in Figs. 2 and 3. (a) Mode with negative azimuthal velocity at $\mu = -0.3$, Re $= 1400$, $m = 1$, Ri $= 25$. (b) Centrifugal-type mode destabilized by viscosity beyond the Rayleigh line, at $\mu = 0.375$, Re $= 5000$, $m = 1$, Ri $= 0.25$. Solid and dashed curves: same as in Figs. 6 and 7. Turning points r_t, as defined in Fig. 6, are shown, but critical points $r_c^{\pm}$, as defined in Fig. 7, are outside the domain in both (a) and (b).

of the CI found in the previous section. The only noticeable difference is the presence of a turning point (as defined in the previous section) exactly where $|w| = 0$, suggesting the mode may extract its energy from the base flow at the critical

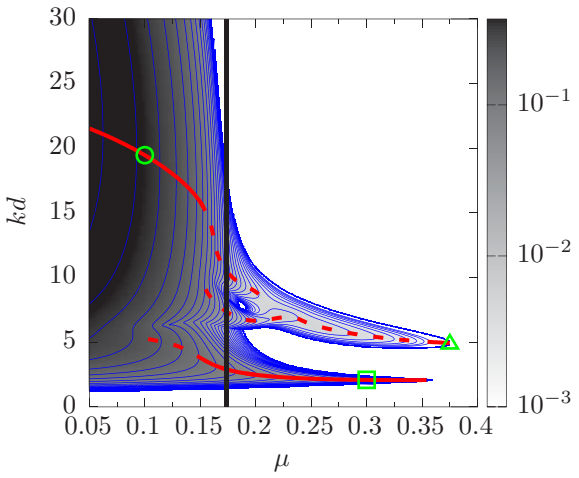

FIG. 9. Positive growth rate contours (with $\Delta \log_{10} \omega_i/\Omega_i = 0.1$) in the (μ,k) plane for Re $= 5000$, Ri $= 0.25$, and $m = 1$. The Rayleigh line $\mu = \eta^2$ is indicated with a solid vertical line. Values of k corresponding to local maxima of the growth rate at the given μ are indicated with thick dashed curves, becoming solid when the maximum is global.

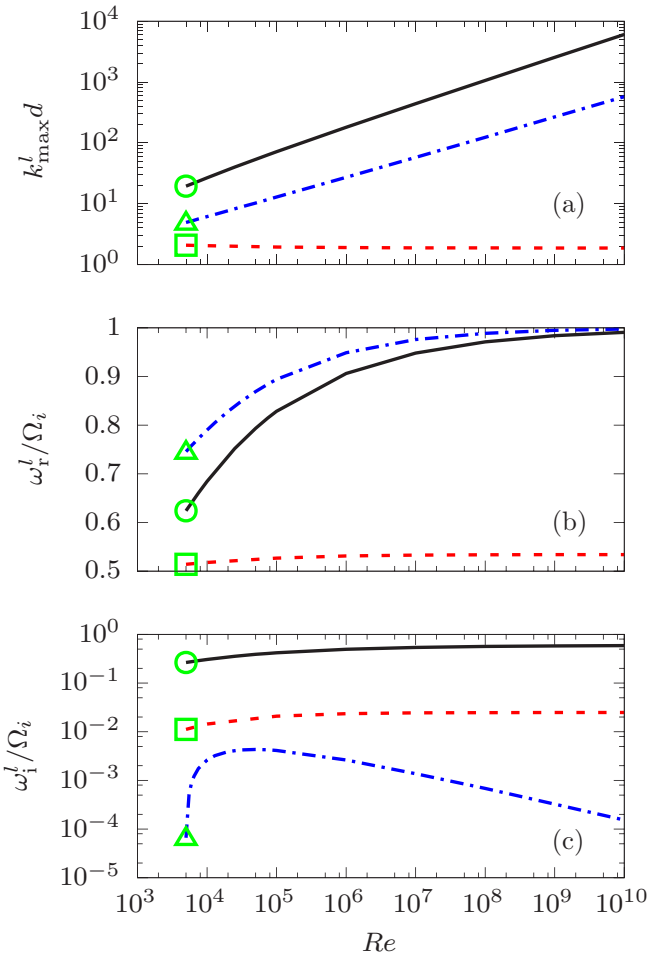

FIG. 10. Evolution of (a) the local optimal axial wave number $k^l_{\max}$ and (b) its associated frequency ω^l_r and (c) growth rate ω^l_i versus Reynolds number for fixed $\mu = 0.1$ (solid line), $\mu = 0.3$ (dashed line), and $\mu = 0.375$ (dash-dotted line); Ri $= 0.25$ and $m = 1$. The wave number $k^l_{\max}$ maximizes the growth rate globally when Re $=$ 5000 (cf. Fig. 9).

layer, as in the RI. In order to determine whether the mode is centrifugal or radiative, we plot isocontours of the growth rate in the (μ,k) plane in Fig. 9. The local maxima of the growth rate in that plane are indicated with dashed red curves, becoming solid when the maximum is global. The plot shows that the dominant (only) instability at $\mu = 0.375$ is created by the merging of two local maxima present in the "centrifugally unstable region" $\mu < \eta^2$. This may explain why the mode is reminiscent of both CI and RI.

Pursuing this further, the three distinct branches, respectively dominating at $\mu = 0.1$, 0.3, and 0.375, are followed as Re $\to \infty$ in Fig. 10. Each branch is a global maximum of $\omega_i(k)$ at Re $= 5000$ and its respective value of μ, but only a local maximum at larger Re, hence the superscript l to denote the associated $k_{\max}$, ω_r, and ω_i. In Fig. 10, we observe very similar trends for the evolution of $k^l_{\max}$ and ω^l_r between the unknown mode at $\mu = 0.375$ and the CI at $\mu = 0.1 < \eta^2$. Indeed, in both cases, $k^l_{\max} \to \infty$ and $\omega^l_r/\Omega_i \to 1$. Both trends were predicted analytically for $(m = 1)$ inviscid CI by Ref. [4], and that $k_{\max}$ remains finite and $\omega_r/\Omega_i < 1$ for the RI [6]. This suggests that

the mode dominating at $(\mu,\mathrm{Re}) = (0.375,5000)$ connects with CI at large Re, despite being outside the so-called centrifugally unstable region. This observation does not contradict the theory in Ref. [4] as the growth rate of this mode tends to zero in the inviscid limit. The conclusion is therefore that this mode is a mixture between a CI and a RI mode, destabilized beyond the Rayleigh line by the joint effects of stratification and viscosity.

Our numerical results suggest that this intrusion of CI-type mode features beyond the Rayleigh line is only possible for nonaxisymmetric modes. That *inviscid* axisymmetric modes still cannot exist beyond the Rayleigh line with stable stratification follows from a simple extension of Rayleigh criterion (see Appendix A). A stronger result can be proved that no *finite-amplitude* axisymmetric state beyond the simple base flow can exist past the Rayleigh line for a viscous, stratified fluid in the thin-gap limit $\eta \to 1$ (see Appendix B). But whether a general proof exists for finite curvature, viscosity, and stable stratification is unclear.

V. CONCLUSIONS

In this paper, we have performed a thorough linear stability analysis of (axially) stably stratified viscous Taylor-Couette flow motivated by ongoing experiments [15–17]. We considered both a large-gap $\eta = 0.417$ and a small-gap $\eta = 0.9$ configuration and varied the rotation ratio μ, the Reynolds number Re, and the Richardson number Ri. This paper bridges the gap between the numerous inviscid analyses of the centrifugal, stratorotational, and radiative instabilities, and the computations of instability thresholds in the viscous case, by addressing the question of the dominant instability mechanism at finite Re beyond the marginal stability line.

As in previous studies, we found that the first bifurcation as Re increases above the marginal curve is always oscillatory, and usually nonaxisymmetric. We showed that the oscillatory $m = 0$ mode is created by a collision between steady Taylor vortex branches. This is an effect of viscosity and stratification (and large Sc too, according to Refs. [18,21]), as this collision disappears at large Re or for $\mathrm{Ri} \neq 0$.

By exploring the discontinuities in the optimal axial wave number $k_{\max}$, we were able to establish a continuous connection between CI and SRI in the (μ,Re) plane. Indeed the optimal wave number $k_{\max}$ diverges for CI in the inviscid limit, whereas it remains finite for the SRI: as a consequence, there exists a value of $\mu \lesssim \eta^2$ where the growth rates of both instabilities are equal. This leads to a discontinuity in $k_{\max}$ at $\mathrm{Re} \to \infty$ which can be tracked down to finite Re, where it eventually disappears as the two local maxima of $\omega_i(k)$ merge into one. The coalescence occurs within the instability region, so it is impossible to distinguish CI from SRI at onset. This explains why Ref. [13] observed a smooth evolution of nonaxisymmetric patterns from the quasi-Keplerian to the centrifugally unstable region in their experiment, whereas Ref. [6] considered the two instabilities distinct in the inviscid limit. As argued in Ref. [6], CI is indeed stronger than SRI when the two instabilities compete in the inviscid limit, but the discontinuity in $k_{\max}$ bends back towards low values of μ as Re diminishes, making SRI dominant over a large portion of the Rayleigh-unstable domain, until the two instabilities can no longer be distinguished. We also established a connection between CI and RI induced by viscosity, without taking the limit of infinite gap as in Ref. [6].

In the unstratified case, we did not expect to find similar discontinuities in $k_{\max}$ for $m \neq 0$, as SRI is a resonance between boundary-trapped inertia-gravity waves. However, we did find two different branches competing in the vicinity of the Rayleigh line for a given $m \neq 0$ when $\mathrm{Ri} = 0$. Each of the competing branches corresponds to a wall mode, localized either at the inner or the outer boundary. These are reminiscent of the two families of branches giving birth to SRI as they interact when $\mathrm{Ri} \neq 0$ [7]. But here the outer-wall mode becomes unstable under the effect of viscosity, not because of a coupling with the inner-wall mode. This outer-wall CI mode, continuously connected to SRI as connected to SRI as $\mathrm{Ri} \neq 0$, was previously unknown because it is always subdominant, yet it is destabilized at finite Re and large-gap widths.

We have also found a dominant $m = 1$ mode propagating against the rotation of the inner cylinder in the counter-rotating strongly stratified case. This behavior has not been reported before, for either one of the three instabilities studied in this paper, since they all require $0 \leqslant \omega_r/m < \Omega_i$ to be able to extract energy from the base flow when $\mathrm{Re} \to \infty$. This is another surprising effect of viscosity on the instability mechanism, since this mode is only dominant at low enough Re.

Finally, we investigated the nature of an $m = 1$ mode dominating beyond the Rayleigh line in the weakly stratified case. This mode seems to have a critical layer, but since its maximum amplitude peaks at the inner cylinder only, it is reminiscent of a radiative mode. However, it shares features of CI rather than RI modes as $\mathrm{Re} \to \infty$. In particular, the optimal wave number diverges while the azimuthal phase speed tends to the inner cylinder angular velocity: two properties of CI. This, however, does not violate the generalized Rayleigh criterion of Ref. [4] as the growth rate asymptotes zero in the inviscid limit. At finite Re, this mode seems connected to both CI and RI in the (μ,k) plane; therefore, we conclude that it is a mixture of CI and RI, destabilized beyond the Rayleigh line by the coupled effects of viscosity and stratification. This reiterates that viscosity has a more complex impact on the stability properties beyond just expected stabilization.

For $\eta = 0.9$, we did not systematically investigate the discontinuities of $k_{\max}$ in the (μ,Re) plane. None were found for both $m = 1$ and $m = 2$ at $\mathrm{Ri} = 0.25$ in the range $\mathrm{Re} < 1 \times 10^4$ but, since a discontinuity must be present near the Rayleigh line in the inviscid limit, we conclude that these discontinuities form at larger Re as $\eta \to 1$. This makes the distinction between SRI and CI types even more problematic and indicates that the effect of viscosity is heightened by reducing the gap size. We also produced dominance diagrams at a lower value of the Schmidt number $\mathrm{Sc} = 7$, in the large-gap case, for $\mathrm{Ri} = 4$ and 25, which are qualitatively similar to $\mathrm{Sc} = 700$ and so not included. The Sc number effects are expected to occur at even lower values of Sc, according to Refs. [18,21].

We conclude by assessing the relevance of the Rayleigh line: even though nonaxisymmetric centrifugal-type modes seem to be able to grow beyond $\mu = \eta^2$ with the help of viscosity and stratification, this limit appears to remain

impassable to axisymmetric ones (whether steady or oscillatory). We were able to prove this result in two distinct limits: inviscid linear disturbances in a finite gap and viscous finite-amplitude disturbances in a thin gap. Whether a more general result suggested by our numerical results (and previous studies) can be proven remains an interesting question.

ACKNOWLEDGMENTS

This work has been supported by the EPSRC (C.L.), under Grant No. EP/K034529/1, and École Normale Supérieure de Paris (F.N.). We thank Stéphane Le Dizès for stimulating discussions.

APPENDIX A: RAYLEIGH CRITERION FOR STABLY STRATIFIED INVISCID FLOW

The Euler equations linearized around the basic flow $\mathbf{U} := r\Omega(r)\hat{\boldsymbol{\theta}}$ [Eqs. (5)–(9) with $\mathrm{Re}\to\infty$] for an axisymmetric ($m=0$) incompressible disturbance can be reduced down to a second-order differential equation for u, the radial perturbation velocity,

$$\frac{d}{dr}\frac{1}{r}\frac{d(ru)}{dr} = \frac{k^2(s^2-\Phi(r))}{s^2-\mathrm{Ri}^*}u \quad \text{where} \quad \Phi := \frac{1}{r^3}\frac{d(r^2\Omega)^2}{dr} \tag{A1}$$

is the Rayleigh discriminant ([22], p. 69). Multiplying by ru^* (where u^* is the complex conjugate of u) and integrating from r_i to r_o gives

$$-\int_{r_i}^{r_o}\frac{1}{r}\left|\frac{d(ru)}{dr}\right|^2 dr = \frac{k^2s^2}{s^2-\mathrm{Ri}^*}\int_{r_i}^{r_o} r|u|^2\,dr - \frac{k^2}{s^2-\mathrm{Ri}^*}\int_{r_i}^{r_o} r\Phi(r)|u|^2\,dr \tag{A2}$$

since $u(r_i)=u(r_o)=0$. Rearranging

$$s^2 = \frac{\mathrm{Ri}^*\int_{r_i}^{r_o}\frac{1}{r}\left|\frac{d(ru)}{dr}\right|^2 dr + k^2\int_{r_i}^{r_o} r\Phi(r)|u|^2\,dr}{\int_{r_i}^{r_o}\frac{1}{r}\left|\frac{d(ru)}{dr}\right|^2 dr + k^2\int_{r_i}^{r_o} r|u|^2\,dr}, \tag{A3}$$

and so providing $\Phi(r)>0$ for all $r\in(r_i,r_o)$, i.e., the basic flow is Rayleigh-stable, then all of the integrals are positive definite which implies $s_i=0$ and stability for all k.

APPENDIX B: UNIQUENESS OF AXISYMMETRIC STATES BEYOND THE RAYLEIGH LINE IN THE THIN GAP LIMIT

Here we prove that the only *streamwise-independent* state that can exist in rotating, stably stratified plane Couette flow beyond the Rayleigh line is one of simple shear, implying that no other axisymmetric state beyond the base state can exist beyond the Rayleigh line in thin-gap stratified Taylor-Couette flow. The proof is a straightforward extension of the unstratified result presented in Ref. [23] to include stratification. In a rotating frame $\Omega=\Omega\hat{\mathbf{z}}$ where the shearing boundaries are at $y=\pm1$ and gravity $\mathbf{g}:=-g\hat{\mathbf{z}}$, there is the simple shear solution $\mathbf{U}=y\hat{\mathbf{x}}$, $P=-\Omega y^2+\frac{1}{2}\mathrm{Ri}\,z^2$, and $\overline{\rho}=-z$ (stable stratification). Rayleigh criterion in this context is that centrifugal instability is only possible for $\Omega<\frac{1}{2}$ (e.g., see Ref. [24]). The governing equations for disturbances away from this steady state ($\mathbf{u}:=\mathbf{u}_{\mathrm{tot}}-\mathbf{U}, p:=p_{\mathrm{tot}}-P, \rho:=\rho_{\mathrm{tot}}-\overline{\rho}$) are

$$\partial_t\mathbf{u} + 2\Omega\hat{\mathbf{z}}\times\mathbf{u} + y\partial_x\mathbf{u} + v\hat{\mathbf{x}} + \mathbf{u}\cdot\boldsymbol{\nabla}\mathbf{u} = -\boldsymbol{\nabla}p - \mathrm{Ri}\,\rho\,\hat{\mathbf{z}} + \frac{1}{\mathrm{Re}}\nabla^2\mathbf{u}, \tag{B1}$$

$$\partial_t\rho + y\partial_x\rho - w + \mathbf{u}\cdot\boldsymbol{\nabla}\rho = \frac{1}{\mathrm{Re}\,\mathrm{Sc}}\nabla^2\rho, \qquad \boldsymbol{\nabla}\cdot\mathbf{u}=0. \tag{B2}$$

Defining $\langle(\cdot)\rangle := \frac{1}{2L}\int_0^L\int_{-1}^1(\cdot)\,dy\,dz$ and $\mathbf{u}=u\hat{\mathbf{x}}+v\hat{\mathbf{y}}+w\hat{\mathbf{z}}$, then for streamwise-independent velocity and density fields taking $\langle u\hat{\mathbf{x}}\cdot(B1)\rangle$, $\langle(v\hat{\mathbf{y}}+w\hat{\mathbf{z}})\cdot(B1)\rangle$ and $\langle\rho(B2)\rangle$ leads to the "energy" integrals

$$\left\langle\frac{1}{2}u^2\right\rangle_t = (2\Omega-1)\langle uv\rangle - \frac{1}{\mathrm{Re}}\langle|\boldsymbol{\nabla}u|^2\rangle, \tag{B3}$$

$$\left\langle\frac{1}{2}(v^2+w^2)\right\rangle_t = -2\Omega\langle uv\rangle - \mathrm{Ri}\langle\rho w\rangle - \frac{1}{\mathrm{Re}}\langle|\boldsymbol{\nabla}v|^2+|\boldsymbol{\nabla}w|^2\rangle, \tag{B4}$$

$$\left\langle\frac{1}{2}\rho^2\right\rangle_t = \langle\rho w\rangle - \tfrac{1}{\mathrm{Re}\,\mathrm{Sc}}\langle|\boldsymbol{\nabla}\rho|^2\rangle, \tag{B5}$$

where periodicity across $z\in[0,L]$ and either nonslip or stress-free velocity fields together with either Dirichlet ($\rho=0$) or Neumann conditions ($\partial_n\rho=0$) for the density on $y=\pm1$ kill all boundary terms which arise. Importantly, all the cubic nonlinear terms drop in these equations and so the kinetic energy in the u field can be treated separately from that in v and w. As a result, generalized energy and dissipation functionals can be constructed as follows:

$$E_\lambda := \frac{1}{2}\langle\lambda^2u^2+v^2+w^2+\mathrm{Ri}\rho^2\rangle, \tag{B6}$$

$$D_\lambda := \langle\lambda^2|\boldsymbol{\nabla}u|^2+|\boldsymbol{\nabla}v|^2+|\boldsymbol{\nabla}w|^2+\frac{\mathrm{Ri}}{\mathrm{Sc}}|\boldsymbol{\nabla}\rho|^2\rangle. \tag{B7}$$

Then $\lambda^2(\mathrm{B3})+(\mathrm{B4})+\mathrm{Ri}(\mathrm{B5})$ gives

$$\frac{dE_\lambda}{dt} = D_\lambda\left\{\frac{[\,2\Omega(\lambda^2-1)-\lambda^2\,]\langle uv\rangle}{D_\lambda} - \frac{1}{\mathrm{Re}}\right\}, \tag{B8}$$

and monotonic decay of the disturbance energy is ensured if

$$\frac{1}{\mathrm{Re}} > \max_{u,v,w,\rho}\frac{[\,2\Omega(\lambda^2-1)-\lambda^2\,]\langle\,uv\,\rangle}{\langle\,\lambda^2|\boldsymbol{\nabla}u|^2+|\boldsymbol{\nabla}v|^2+|\boldsymbol{\nabla}w|^2+\frac{\mathrm{Ri}}{\mathrm{Sc}}|\boldsymbol{\nabla}\rho|^2\,\rangle}$$

for any real λ. The maximum on the right-hand side can be minimized over λ to give the best energy stability result. Clearly, $\rho=0$ is a feature of the optimizer and we can rescale u by defining $\phi:=-\lambda u$ to get an expression for the energy stability Reynolds number Re_E as

$$\frac{1}{\mathrm{Re}_E} := \min_\lambda\frac{\lambda^2-2\Omega(\lambda^2-1)}{\lambda} \times \max_{\phi,v,w}\frac{\langle\phi v\rangle}{\langle|\boldsymbol{\nabla}\phi|^2+|\boldsymbol{\nabla}v|^2+|\boldsymbol{\nabla}w|^2\rangle},$$

where the implication is that *all* streamwise disturbances decay for $\mathrm{Re} < \mathrm{Re}_E$ regardless of their amplitude. The latter maximization corresponds to $1/\mathrm{Re}_E$ for an unstratified, nonrotating layer where $\mathrm{Re}_E = \frac{1}{2}\sqrt{1708} \approx 20.7$ [25] under nonslip conditions. The minimization problem has the minimum $2\sqrt{2\Omega(1-2\Omega)}$ for $0 \leqslant \Omega \leqslant \frac{1}{2}$ and zero otherwise for real λ. As a result, we have

$$\mathrm{Re}_E = \begin{cases} \frac{\sqrt{1708}}{4\sqrt{2\Omega(1-2\Omega)}}, & 0 < \Omega < \frac{1}{2} \\ \infty, & \Omega \leqslant 0 \text{ or } \Omega \geqslant \frac{1}{2}. \end{cases}$$

So, on and beyond the Rayleigh line $\Omega = \frac{1}{2}$, the (generalized) energy of all streamwise-independent disturbances, *regardless of their amplitude*, monotonically decays in time *for any* Re. To guarantee that $E_\lambda \to 0$ (and hence the ultimate vanishing of all disturbance fields), we need a Poincaré inequality $E_\lambda < \alpha D_\lambda$ for some $\alpha = \alpha(L)$ so that Eq. (B8) becomes $dE_\lambda/dt < -\beta^2 E_\lambda$ for some constant β. Grönwall's inequality then gives the required result. A Poincaré inequality exists for nonslip conditions on the velocity field and either Dirichlet or Neumann conditions on the density field (in the latter case only if no mean flow is allowed in the direction of gravity). (Note that once $\mathrm{Re} = 177.2$ for any Ω, two-dimensional *spanwise-invariant* disturbances are not assured to decay [23] so that there is no general global stability result for the basic state beyond the Rayleigh line.)

[1] M. J. Molemaker, J. C. McWilliams, and I. Yavneh, Phys. Rev. Lett. **86**, 5270 (2001).
[2] I. Yavneh, J. C. McWilliams, and M. J. Molemaker, J. Fluid Mech. **448**, 1 (2001).
[3] L. Rayleigh, Proc. R. Soc. London Ser. A **93**, 148 (1917).
[4] P. Billant and F. Gallaire, J. Fluid Mech. **542**, 365 (2005).
[5] B. Dubrulle, L. Marié, C. Normand, D. Richard, F. Hersant, and J.-P. Zahn, Astron. Astrophys. **429**, 1 (2005).
[6] S. Le Dizès and X. Riedinger, J. Fluid Mech. **660**, 147 (2010).
[7] J. Park and P. Billant, J. Fluid Mech. **725**, 262 (2013).
[8] E. M. Withjack and C. F. Chen, J. Fluid Mech. **66**, 725 (1974).
[9] B. M. Boubnov, E. B. Gledzer, and E. J. Hopfinger, J. Fluid Mech. **292**, 333 (1995).
[10] B. M. Boubnov, E. B. Gledzer, E. J. Hopfinger, and P. Orlandi, Dyn. Atmos. Oceans **23**, 139 (1996).
[11] F. Caton, B. Janiaud, and E. J. Hopfinger, Phys. Rev. Lett. **82**, 4647 (1999).
[12] F. Caton, B. Janiaud, and E. J. Hopfinger, J. Fluid Mech. **419**, 93 (2000).
[13] M. Le Bars and P. Le Gal, Phys. Rev. Lett. **99**, 064502 (2007).
[14] J. Park and P. Billant, Phys. Fluids **25**, 086601 (2013).
[15] C. Leclercq, J. L. Partridge, P. Augier, S. B. Dalziel, and R. R. Kerswell, J. Fluid Mech. **791**, 608 (2016).
[16] C. Leclercq, J. L. Partridge, P. Augier, C. P. Caulfield, S. B. Dalziel, and P. F. Linden, arXiv:1609.02885.
[17] C. Leclercq, J. L. Partridge, C. P. Caulfield, S. B. Dalziel, and P. F. Linden, arXiv:1609.02886.
[18] S. A. Thorpe, in *Notes on 1966 Summer Study Program in Geophysical Fluid Dynamics at the Woods Hole Oceanographic Institution*, Vol. II: Fellowship Lectures, edited by M. C. Thayer and W. V. R. Malkus (Summer School, Woods Hole, MA, 1966), pp. 80–110.
[19] D. Shalybkov and G. Rüdiger, Astron. Astrophys. **438**, 411 (2005).
[20] G. Rüdiger and D. A. Shalibkov, Astron. Astrophys. **493**, 375 (2009).
[21] B. L. Hua, S. Le Gentil, and P. Orlandi, Phys. Fluids **9**, 365 (1997).
[22] P. G. Drazin and W. H. Reid, *Hydrodynamic Stability* (Cambridge University Press, Cambridge, 1981).
[23] W. L. Hung, D. D. Joseph, and B. R. Munson, J. Fluid Mech. **51**, 593 (1972).
[24] F. Rincon, G. I. Ogilvie, and C. Cossu, Astron. Astrophys. **463**, 817 (2007).
[25] D. D. Joseph and B. R. Munson, J. Fluid Mech. **43**, 545 (1970).